Ultra low-loss, isotropic 2D optical negative-index metamaterial based on hybrid metal-semiconductor nanowires

R. Paniagua-Domínguez, D. R. Abujetas, and J. A. Sánchez-Gil

Instituto de Estructura de la Materia, Consejo Superior de Investigaciones Científicas
Serrano 121, 28006 Madrid, Spain

January 25, 2013

1 Scattering and extinction efficiency of electromagnetic waves from a coated cylinder

Here we detail the scattering and extinction efficiencies from a coated cylinder under normal plane wave illumination. Let us fix the polarization of the incident wave to be such that the magnetic field is directed along the axis of the cylinder (TE-polarization). Consider two concentric cylinders of radii R_{int} and R_{out}, and permittivities $\epsilon_c = m_c^2$ and $\epsilon_s = m_s^2$, respectively, the extinction and scattering efficiencies can be expressed as [1]:

$$Q_{sca} = \frac{2}{x}(|a_0|^2 + 2\sum_{n=1}^{\infty}|a_j|^2) \tag{1}$$

$$Q_{ext} = \frac{2}{x}Re(a_0 + 2\sum_{n=1}^{\infty}a_j) \tag{2}$$

with

$$a_n = \frac{\begin{vmatrix} 0 & J_n^{'}(k_sR_{int}) & H_n^{'}(k_sR_{int}) & J_n^{'}(k_cR_{int}) \\ 0 & m_sJ_n(k_sR_{int}) & m_sH_n(k_sR_{int}) & m_cJ_n(k_cR_{int}) \\ J_n^{'}(k_0R_{out}) & J_n^{'}(k_sR_{out}) & H_n^{'}(k_sR_{out}) & 0 \\ m_0J_n(k_0R_{out}) & m_sJ_n(k_sR_{out}) & m_sH_n(k_sR_{out}) & 0 \end{vmatrix}}{\begin{vmatrix} 0 & J_n^{'}(k_sR_{int}) & H_n^{'}(k_sR_{int}) & J_n^{'}(k_cR_{int}) \\ 0 & m_sJ_n(k_sR_{int}) & m_sH_n(k_sR_{int}) & m_cJ_n(k_cR_{int}) \\ H_n^{'}(k_0R_{out}) & J_n^{'}(k_sR_{out}) & H_n^{'}(k_sR_{out}) & 0 \\ m_0H_n(k_0R_{out}) & m_sJ_n(k_sR_{out}) & m_sH_n(k_sR_{out}) & 0 \end{vmatrix}} \tag{3}$$

In these expressions, m_0, m_s and m_c are the refractive indices of the external medium, the shell and the core, respectively. The same holds for k, the wavenumber. J_n and H_n are the Bessel and Hankel functions.

2 Low loss isotropic 2D negative-index metamaterial based on a square lattice of Silver-Germanium core-shell nanocylinders

Let us next study the case of a square lattice of Ag@Ge core-shell nanowires. Since the square lattice possesses lower symmetry than the hexagonal, it would not be surprising to find some degree of anisotropy. In Fig.1, we have plotted the magnetic and electric contributions to the scattering, together with the total efficiency, for core-shell nanowires of outer radius $R_{out} = 170$ nm as a function of the wavelength of incidence and inner radius (R_{int}). The electric and magnetic responses spectrally overlap over a relatively wide range, $\lambda_0 \sim (1200, 1500)$ nm, for R_{int} values between 60 and 100 nm. In Fig.2(a) we have plotted, specifically, the optical properties of a Ag@Ge core-shell nanowire with external radius $R_{out} = 170$ nm and internal radius $R_{int} = 90$ nm. For this nanostructure there is a spectral overlap between the electric and magnetic resonances for $\lambda_0 \in (1300, 1500)$ nm. We have also performed full numerical simulations for this system, considering several slabs with different thicknesses obtained by arranging these nanowires in a simple square lattice with lattice period $L = 350$ nm, thus keeping fixed the surface-to-surface distance between neighbouring particles ($d_{s-s} = 10$ nm): this leads to filling fractions of $f \sim 0.74$. Therefore, we expect to achieve lower absolute values of the real part of the index.

In Figure 2(b), the obtained transmission spectra under normal incidence illumination are depicted. The frequency window in which propagation is allowed presents Fabry-Perot modes. For this square lattice arrangement, typically, $N-1$ peaks are present along the propagation direction. The transmission peak arising at higher energies ($\lambda \sim 1175$ nm), related to the electric-quadrupole-like mode, disappears for sufficiently thick slabs, as evidenced in the 45 u.c.-thick slab case (see

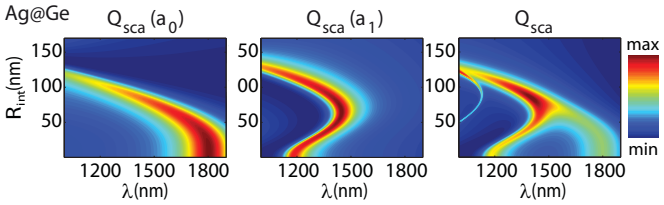

Figure 1: Magnetic (left) and dipolar electric (centre) contributions to the total scattering efficiency (right) of a 170 nm Ag@Ge core-shell nanocylinder.

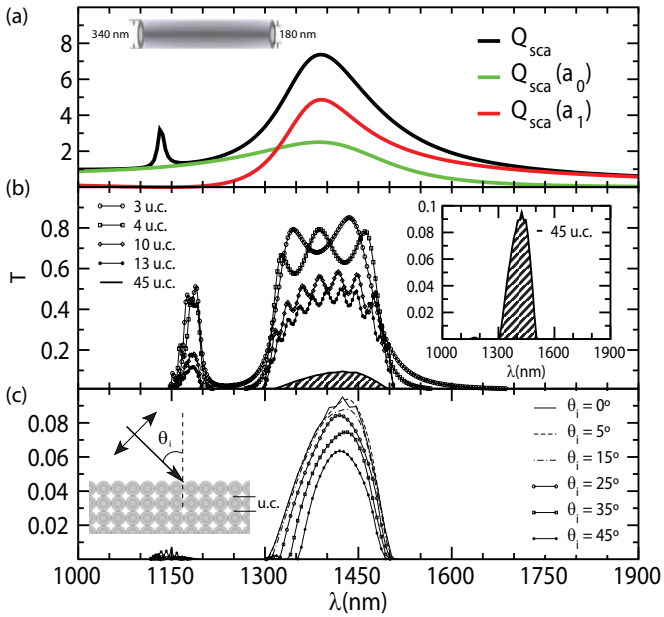

Figure 2: (a) Scattering efficiency for a Ag@Ge core-shell nanowire with external radius $R_{out} = 170$ nm and internal radius $R_{int} = 90$ nm. The contributions of the two first terms in the expansion of the field are also shown. (b) Transmission curves through metamaterial slabs of several thicknesses under normal incidence illumination. The slabs are obtained by arranging these core-shell nanowires periodically in a square lattice (period $L = 350$ nm). Curves with different symbols represent different slab thicknesses. The inset shows the case of a slab with a thickness of 45 unit constituents (u.c.). (c) Transmission curves through a 45 u.c-thick slab under several angles of incidence.

the inset in Fig.2(b)). Therefore, we expect the refractive index of the metamaterial to be negative in this transmission window, with low associated losses, although slightly higher than in the Ag@Si case (notice that the same transmission is present in the $N = 45$ case for the Ag@Ge nanowires than in the $N = 60$ case for the Ag@Si structures, which implies a propagation length inside the NIM of about 16 μm, compared to the 21 μm obatined fo the Ag@Si). Several angles of illumination, θ_i have been considered. The results obtained for the 45 u.c.-thick slab and $\theta_i \in (0°, 45°)$ are shown in Fig.2(c). For low angles of incidence, $\theta_i \in (0°, 25°)$, transmission curves are almost identical. However, for high enough angles of incidence, $\theta_i \in (25°, 45°)$ there is a narrowing of the transmission window in the high frequency limit. As will be shown later, in that region the real part of the effective index of refraction (n_{eff}) reaches its lowest values (even approaching zero, $|Re(n_{eff})| \sim 0$). For those wavelengths for which the transmission suddenly drops, the incidence angles are above corresponding critical angles for total internal reflection. Therefore, no transmission is allowed. This allows for an alternative way to determine the real part of the index. In the lower panel of Fig.3, results for $Re(n_{eff})$ obtained from simulations within the transmission window are depicted. The blue dashed curve represents the obtained values from S-parameter retrieval procedures. Red squares are the obtained values from Snell's law applied to a 30 u.c.-thick slab under $\theta_i = 10°$ illumination. Black circles are the values retrieved from the simulation of a rectangular prism with an angle $\theta_{prism} \sim 26.5°$. Additionally, the transmission curves under oblique incidence, in which the incident wave experiences total internal reflection, enables to obtain $Re(n_{eff})$ at the wavelength for which $T = 0$, by simply applying $Re(n_{eff}) = -sin(\theta_i)$ (green diamonds in Fig.3). The retrieved values for $Re(n_{eff})$ seem to be consistent regardless of the angle of incidence, even though one could expect the system to present anisotropy. Error bars in those results stemming from the application of Snell's law have been estimated assuming, a systematic error of $\pm 2°$ in the determination of the angle. As expected, absolute values of the index of refraction are lower as compared with the Ag@Si in the hexagonal lattice, due to the lower value of the filling fraction. However, NIM behaviour with $n_{eff} \sim -1$ is clearly observed. Although higher in this case (see upper panel of figure 3), losses are still very low. At $\lambda \sim 1390$ nm, for which $Re(n_{eff}) = -1$, the f.o.m. reaches 4.7, implying an imaginary part of the index of only $Im(n_{eff}) = 0.21$.

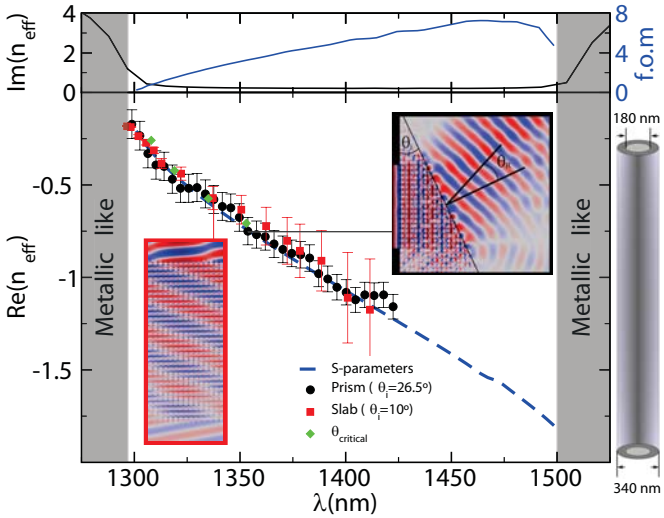

Figure 3: Lower Panel: Retrieved real part of the index of refraction using Snell's law for a metamaterial built with Ag@Ge core-shell nanowires with $R_{int} = 90$ nm and $R_{out} = 170$ nm arranged in a square lattice. The blue discontinuous curve represents the values obtained from complex reflection and transmission coefficients of a 45 u.c.-thick slab under normal incidence. Black circles represent the retrieved values from Snell's law in the prism configuration. The incidence angle is fixed, $\theta_i = \theta_{prism} \sim 26.5\,\text{deg}$. The corresponding inset shows the y-component of the electric field (only non-zero of the incident wave) for the particular case $\lambda \sim 1355$ nm. Red squares represent the values obtained from Snell's law in the slab configuration. The angle of incidence is $\theta_i = 10\,\text{deg}$. The corresponding inset represents the x-component (parallel to the first interface) of the electric field for $\lambda \sim 1335$ nm. Green diamonds are the values retrieved from critical angles for total internal reflection. Upper Panel: Imaginary part of the index of refraction obtained from complex reflection and transmission coefficients (black curve) and figure of merit, f.o.m., as defined in the text (blue curve)

3 Influence of Silicon losses

In this section we study the influence of absorption in Silicon in the obtained figure-of-merit of the core-shell NW based metamaterial. In figure 4 we plotted the optical properties of Ag@Si core-shell systems considering Si to be lossless ($n_{Si} = 3.5$, upper panel) and lossy (n_{Si} taken from [3], lower pannel). In both cases Ag material properties taken from [2]. While the resonances stemming from a_0 and a_1 are almost unaffected (in that frequency range the imaginary parti of n_{Si} is extremely low), the higher order resonance gets redshifted, due to the slight dispersion in the real part of n_{Si} and absorption efficiency increases since Si begins to absorb.

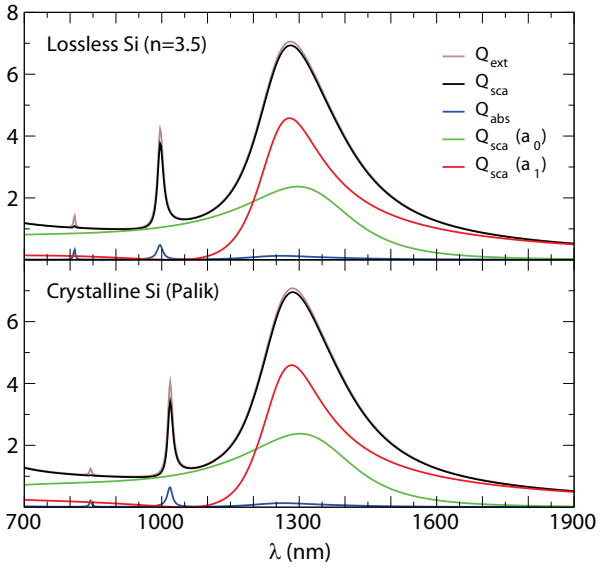

Figure 4: Upper Panel: Optical properties of a Ag@Si core-shell nanowire with external radius $R_{out} = 170$ nm and internal radius $R_{int} = 80$ nm. Si is considered lossless with $n_{Si} = 3.5$ and Ag material properties taken from [2]. Besides the extinction, scattering and absorption efficiencies of the system, contributions of the two first terms in the expansion of the field are also shown. Lower Panel: Same as in the upper panel but with Si material properties taken from [3], including absorption.

We studied the same configuration as in the main text (an hexagonal lattice of these core-shell NWs with a filling fraction of $f \sim 0.856$) with Si material parameters taken from [3]. Results can be found in figure 5. Since Si is very weakly absorbing in this frequency range, values obtained within the negative index window are almost unaffected.

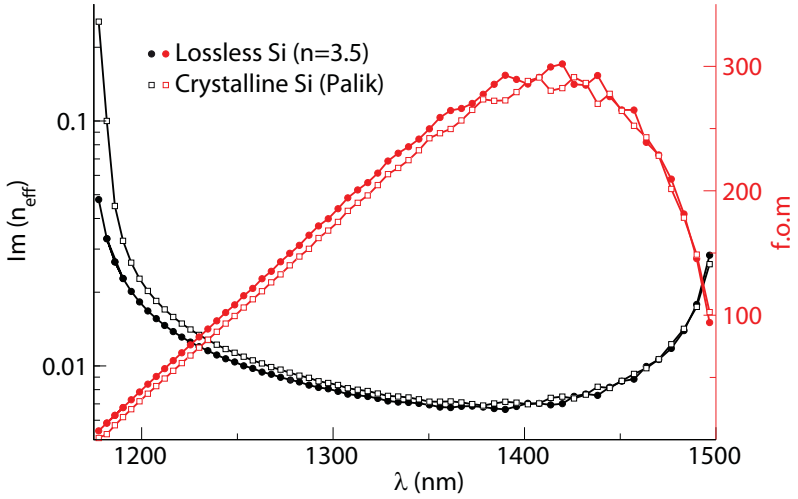

Figure 5: Comparison between the imaginary part of the effective index of refraction, together with the figure-of-merit (f.o.m.), retrieved for a metamaterial made up of Ag@Si core-shell NW with $R_{out} = 170$ nm and $R_{int} = 80$ nm arranged in a hexagonal lattice with $f \sim 0.856$, in the cases of lossless Si ($n_{Si} = 3.5$) and n_{Si} taken from [3]

References

[1] Kerker, M. and Matijević, E. *J. Opt. Soc. Am.* **51**, 506 (1961).

[2] Johnson, P. B. & Christy, R. W. Optical constants of the noble metals. *Phys. Rev. B* **6**, 4370 (1972).

[3] Palik, E. D. *Handbook of Optical Constants of Solids* (Academic Press, 1998).